

GRAND/AMCS/ N-37

SIMULATION STUDIES FOR SURFACES
AND MATERIALS STRENGTH

74195
CR
139

Semi-Annual Report
for
Cooperative Agreement NCC2-297

for the period
November 1, 1986 - April 30, 1987

Submitted to

National Aeronautics and Space Administration
Ames Research Center
Moffett Field, California 94305

Computational Chemistry Branch
Dr. David Cooper, Chief and Technical Monitor

Thermosciences Division
Dr. Jim Arnold, Chief

Prepared by

ELORET INSTITUTE
3788 Fabian Way
Palo Alto, CA 94303
Phone: 408 730-8422 and 415 493-4710
K. Heinemann, President and Grant Administrator
Timur Halicioglu, Principal Investigator

(NASA-CR-180539) SIMULATION STUDIES FOR
SURFACES AND MATERIALS STRENGTH Semiannual
Report, 1 Nov. 1986 - 30 Apr. 1987 (Eloret
Corp.) 13 p Avail: NTIS HC A02/MP A01

N87-22277

Unclas
CSCL 20K G3/39 0074195

Three different investigations based on computer simulations were carried out during this period. Simulation calculations were performed using model potentials with two- and three-body interactions which were represented by the Mie and the Axilrod-Teller potentials, respectively. In the first part, to analyze stability criteria for simple crystals, a parametrical investigation was carried out and stability regions for five different crystalline structures were determined with respect to potential energy parameters. To simulate some of the basic surface processes such as diffusion and nucleation, in the second and third parts, we considered silicon surfaces as a specific example. In these studies diffusion of adatoms on stepped surfaces were simulated and energetics associated with the formation of kink sites were calculated.

1. Stability Diagrams for Simple Crystals

In simulation calculations structural stability of the model system is an important aspect. Often, it is desired that the structure of the system under consideration corresponds to the energetically most favorable configuration. For a given potential energy function, finding the most stable structure among different possible configurations is a cumbersome and time consuming procedure. This problem emerges, in particular, for potential energy functions involving three-body interactions which furnish stability regions for a large number of crystalline structures ranging from the close-packed (HCP or FCC) to more open (e.g., diamond cubic or β -tin) structures. The significance of three-body interactions in calculating the energy and structure-related properties of simple crystals were shown in our earlier investigations.

In the present study, stability regions for five different crystalline structures (HCP, FCC, BCC, β -tin and diamond cubic) were calculated for a wide range of potential parameters. Calculations were carried out in a dimensionless form using the Mie potential and the Axilrod Teller function to represent two- and three-body interactions, respectively. The results are presented in a graphical form in Figure 1. This representation is found to be very useful in deciding parameters for various specific systems in which two-body and three-body interactions are operational. The stability map shown in Figure 1 represents clearly the effect of the three-body interaction on the stability of crystals. A potential energy function based only on a two-body potential is able to provide stable regions only for HCP and FCC structures. In analyzing Figure 1 one should remember that every point on these maps corresponds to the energetically most stable structures among the five different crystals taken into consideration in this work. The general tendency in the stability of these crystals as a function of Z^* is changing as HCP \rightarrow FCC \rightarrow BCC for small n , as HCP \rightarrow FCC \rightarrow β -tin \rightarrow diamond cubic for intermediate values of n

and as HCP \rightarrow FCC \rightarrow diamond cubic for larger n values. Because of the structural similarities, the difference between energies calculated for HCP and FCC structures turned out to be very small. Within our accuracy limits the HCP and FCC structures were considered energetically degenerate for regions denoted by HF which occupies large areas in the stability maps for $n \leq 6$ (see Figure 1).

Boundaries between the stability regions should not be taken as sharp limits. Due to the discrete nature of the calculations all boundaries must be regarded rather as somewhat broader transition regions. The map for $n = 5$ is interesting; for example for $Z^* = 0.825$ and $m = 9$ all five crystalline structures seem to have a common region. The β -tin structure has a narrow stability region from $n = 5$ to $n = 8$.

2. Adatom Diffusion and Ledge Interactions on the Si(111) Surface

Knowledge concerning the diffusion of atoms on surfaces containing ledges is essential for the proper understanding of crystal growth phenomena at an atomic level. Early studies on metal surfaces revealed the importance of adatom-ledge interactions for surface diffusion when attempting to evaluate different growth mechanisms. Based on calculations of surface structure and energetics for single atoms, the motion of particles across an otherwise flat ideal Si(111) surface will occur by activated jumps between hole sites. These jumps will carry the atom through the cradle sites so that the minimum energy path for the motion of an atom from the hole to the cradle site will control this diffusion process. Figure 2 defines these and other possible adatom positions. Of course, the actual macroscopic process of surface diffusion depends on the detailed structure of the surface so that diffusion via this simple unit process is expected to be somewhat modified by (7×7) , (2×1) or (1×1) surface reconstruction patterns and by the presence of ledges on the surface.

In the present study, the "Constrained Statics" method is utilized to find the minimum energy configuration of the surface when one adatom is constrained to relax only in a specific plane while all other atoms relax in all three dimensions. Many similar computations are performed for the specific atom in different initial positions and minimum energy trajectory which takes the atom from one position to another is thus mapped out. The result for the hole to cradle trajectory is shown in Figure 3. The moving atom stayed in the vertical plane containing the two sites, as expected, so that it passed through the bridge site with an interaction energy of 1.24 eV (see Figure 2), which is clearly an inflection point on the energy trajectory. A small additional energy hump (0.12 eV) exists between the bridge site and the metastable cradle site (0.99 eV). Upon analysis of overall structure when the adatom was near the energy maximum (1.36 eV), the energy hump was seen to be caused by the development of a significant local reconstruction underneath the cradle site.

The subsequent cradle to hole site energy barrier, to complete the overall hole to hole motion, is $E_c = 0.36$ eV.

These are the absolute minimum energy changes that can be associated with the jump. In practice, the large local atomic reconstruction at the cradle site is not likely to happen during an adatom jump so that the hole site to hole site adatom movement could exhibit an average maximum activation energy somewhat greater than 1.36 eV. Experimental estimates for the Si(111) surface diffusion activation barrier range from 0.2 to 2.0 eV due to the very indirect nature of the data which must be analyzed and interpreted, and because of the uncertainty of the local surface structure and composition.

Adatom-Ledge Interactions

Although it is important to study all adatom-ledge interactions, only the hole adatom-[211] ledge interactions are considered here. Figure 4 gives side views of the [211] lower and upper ledges, respectively, displaying the adatom positions tested. Simulation calculations were performed with ledges at 25.45\AA spacings. Figure 4c plots the hole formation energies, E_f , using circles for the lower ledge and squares for the upper ledge. The data points are vertically coincident with their spatial positions in Figures 4a and 4b. The horizontal dashed line shows the formation energy for the adatom at a hole site on the flat ideal surface, labeled as E_f , indicating the energy that would obtain at an infinite distance from the ledge.

From our earlier study, we found that the hole adatom puts the surface further into compression, and that a 0.5% in-plane tensile strain caused the E_f of the hole adatom to decrease (become more favorable) by 0.08 eV. In Figure 4, where the upper ledge causes a major reduction of the surface compression, the hole E_f should be much lower near the edge, as Figure 4c clearly confirms. In fact, the stress effect is larger on the terrace above the ledge than on the lower terrace, and the E_f is also more negative above the ledge. The increase in the adatom energies right next to the ledge is arguably due to the interference of short range reconstruction displacements of the adatoms and ledge which begin to dominate the longer range stress interactions.

The lower [211] ledge has a much smaller effect on the surface compression, but it still decreases it somewhat, particularly on the terrace above the ledge. However, in the explicit calculation of Figure 4, the hole adatom is not at all favored on the upper site of this ledge, and it is repulsed significantly from the terrace below the ledge. It may be that the shear fields may offset the otherwise favorable effect of the normal stresses above the ledge. The repulsion below the ledge does not have any obvious explanation in terms of simple stress interactions. As argued above, the local reconstructions interfering with one another may be the source of repulsion. Or, the stresses in the underlying puckered layers, which have not been extensively analyzed thus far, may be involved in the repulsion effect.

The only firm conclusion to be drawn from these results is that the surface behavior is not always so easily cast into a simple top layer stress interaction model. In the case of the upper ledge, where the stress effect is huge, the stress analysis is sufficient. For the lower ledge, where the surface compression is not a dominant feature, there is no simple correlation between the stress effects of the separate defects and their interaction energy.

Perhaps the most important point to notice about Figure 4 is that the adsorption energies of adatoms near the ledge are symmetrical, an assumption that has been used in most computations of adatom diffusion to ledges via both the lower and upper terraces. Of course, these numbers are expected to change when more adatoms and surface vacancies are present and when the terraces reconstruct into distinctive patterns.

3. Kink-Site formation Energies on the Si(111) Surface

A semiempirical potential energy function (PEF) has been developed for Si comprising both two-body and three-body effective potentials that has significant application to a variety of phenomena ranging from cluster stabilities to crystal growth considerations. The parameters contained in this PEF were obtained from fits to various experimental properties. Using this PEF, as described in our earlier reports, more than 25 different materials properties of Si bulk, clusters and surfaces were successfully reproduced. The calculated energy quantities are all within $\pm 20\%$ while structural properties, such as bond distances for small clusters and the nearest neighbor distance in relaxed crystals, were reproduced to within 7%. However, quantities related to the second derivatives of energy, such as bulk modulus, elastic constants and vibrational properties were not predicted so well and only qualitative agreement is obtained for such parameters. On the other hand, surface energy values for the Si(100), (110) and (111) surfaces were predicted with good precision and the PEF produces the correct surface reconstruction geometry for the (2×1) Si(100) surface and for the (2×1) Si(111) surface.

In the crystal growth, as well as in the surface reconstruction processes, energy values associated with the kink formation are very important. It would be very nice if one could make first principles *ab initio* calculations of surface quantities like ledges and kinks; however, such calculations are only possible for very small systems containing only a few atoms. Since long-range surface stress effects due to interacting ledges on Si(111) surfaces have been calculated and found to be important to make meaningful ledge or kink calculations with any PEF, about 500-1000 atoms must be taken into account. It is for this reason that one is presently limited to the use of semiempirical potential functions. Of the alternate semiempirical Si PEF's available today none has the track record of that proposed here. Each undoubtedly has its strengths and weaknesses but insufficient experience is available to catalogue

their applicability in a given situation. Perhaps it is best to look at each as the analogue of a particular experimental technique that provides a measurement with a certain error bar. Refinement of the technique generally reduces the error bar. Such semiempirical PEF's are able to make a determination of ledge and kink energies which is more than present experimental techniques can do. Granted, one does not really know the magnitude of the error bar generated by using a particular PEF so the number should be treated with caution until substantiated in some alternate fashion; however, it is the best path presently available to determine some quantities important to crystal growth modeling.

Using the present PEF, most recently, the structure and energetics for the dominant ledges on the Si(111) surface have been calculated. These ledges are free of kinks and, therefore, are not the equilibrium configuration except at $0^\circ K$. However, the properties of four different kind of $[2\bar{1}\bar{1}]$ and $[\bar{2}11]$ ledges that can be found on the Si(111) provide a necessary baseline and are an important structural basis for kink formation studies. These four structures are presented in Figure 5. The ledge energy per atom for these four structures at large ledge spacing are $\lambda = 0.24$ and 0.01 eV for $[2\bar{1}\bar{1}]$ lower and upper ledges, respectively, while $\lambda = 0.192$ and 0.01 eV for $[\bar{2}11]$ lower and upper ledges, respectively. This report presents calculations of the kink structure and the kink energetics on these ledges. These kink properties are also expected to depend upon the state of surface reconstruction, either by a direct structural connection or indirectly through the surface stresses. Although the surface reconstruction problem should be attacked first and a more thorough study of ledges in contact with such reconstructed surfaces is needed before the nature of the kink sites can be studied in detail, there is pedagogical value to be gained from a study of kink formation on these $0^\circ K$ ledges. Because of these limitations, only a preliminary study of a few kink sites will be presented here.

Results for isolated kink formation on both the $[2\bar{1}\bar{1}]$ and $[\bar{2}11]$ upper ledges and the $[2\bar{1}\bar{1}]$ lower ledge at $0^\circ K$ are summarized in Figure 6. Although three examples do not constitute a statistically significant trend, the main feature of interest is that the kink formation energy is low when the reconstructed ledge energy is high. The ledge energy is low when the reconstruction produces a large tensile stress component and reduces the net local stress to very small values. Thus, little additional stress relaxation can occur via kink formation. For those ledges that do not reconstruct strongly, kink formation has the opportunity of strongly relaxing the local compressive stress.

Large values of E_k will lead to a small kink density and thus slow ledge movement during crystal growth at a given driving force. Small values of E_k lead to high kink densities and thus rapid ledge movement during growth at such driving force. Thus, although the $[2\bar{1}\bar{1}]$ and $[\bar{2}11]$ ledges will bound the terraces on the Si(111) surface at equilibrium for energetic reasons, they will be the slowest growing ledges and will thus also bound the terraces during crystal growth for kinetic reasons. In

actual practice, the foregoing conclusion is always valid, however, for doped materials interaction energies must be properly modified to obtain correct kink energy values.

Figure Captions

- 1) *Stability regions for five simple crystalline structures, HCP (H), FCC (F), BCC (B), β -tin (S) and Diamond cubic (D). Parameters m and n are the repulsive and attractive exponents of the Mie potential, respectively, while Z^* represents the three-body intensity parameter.*
- 2) *Top view of postulated adatom adsorption sites on the Si(111) surface*
- 3) *Minimum energy path for the motion of an adatom from the hole site to the cradle site. Energies are in eV measured relative to the hole site adatom formation energy.*
- 4) *Formation energies for hole adatoms near the (a) lower and (b) upper $[211]$ ledges. Adatom positions are shown with filled triangles in (a and b). Energies are plotted directly below in (c), using circles for the lower ledge and squares for the upper ledge.*
- 5) *Relaxed structures of the basic $[\bar{2}11]$ and $[2\bar{1}\bar{1}]$ single height ledge on Si(111).*
- 6) *Structures and energies for selected single height ledges (λ_∞) and kink sites (E_k) on Si(111).*

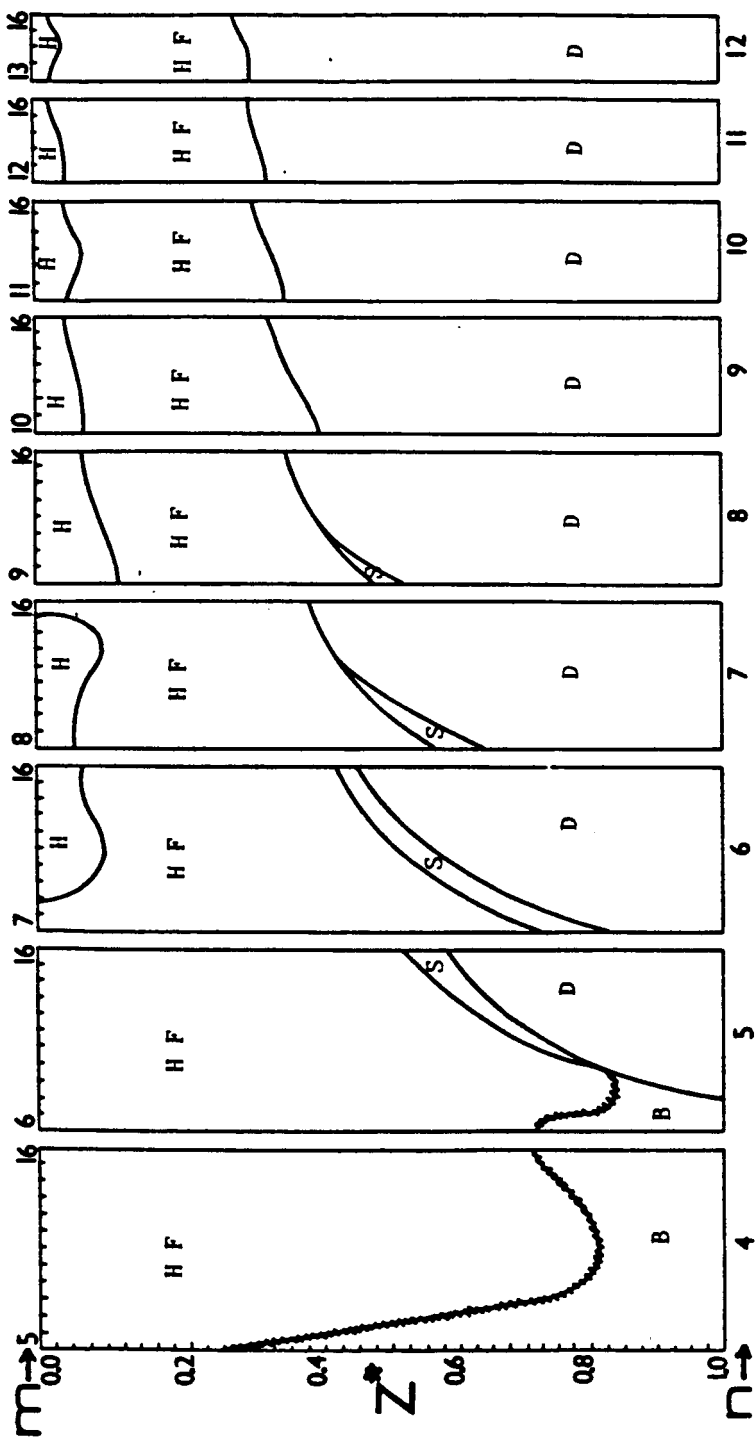


FIGURE 1

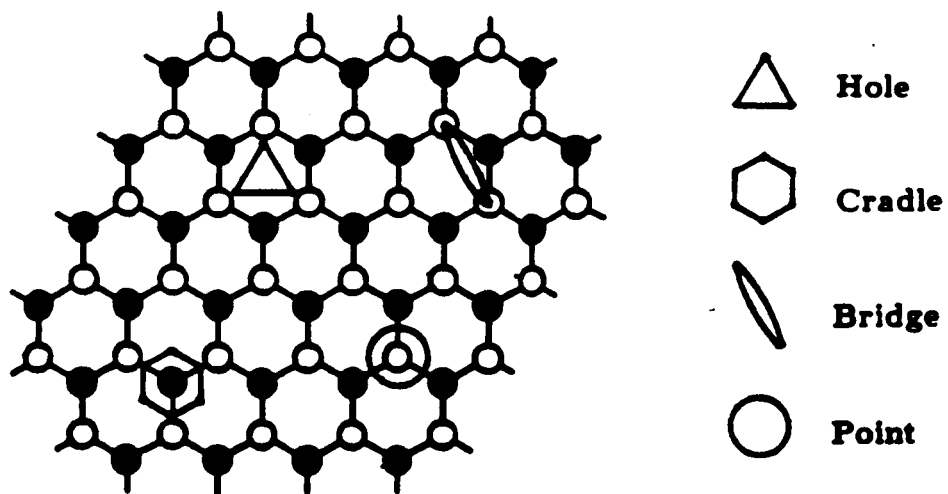


FIGURE 2

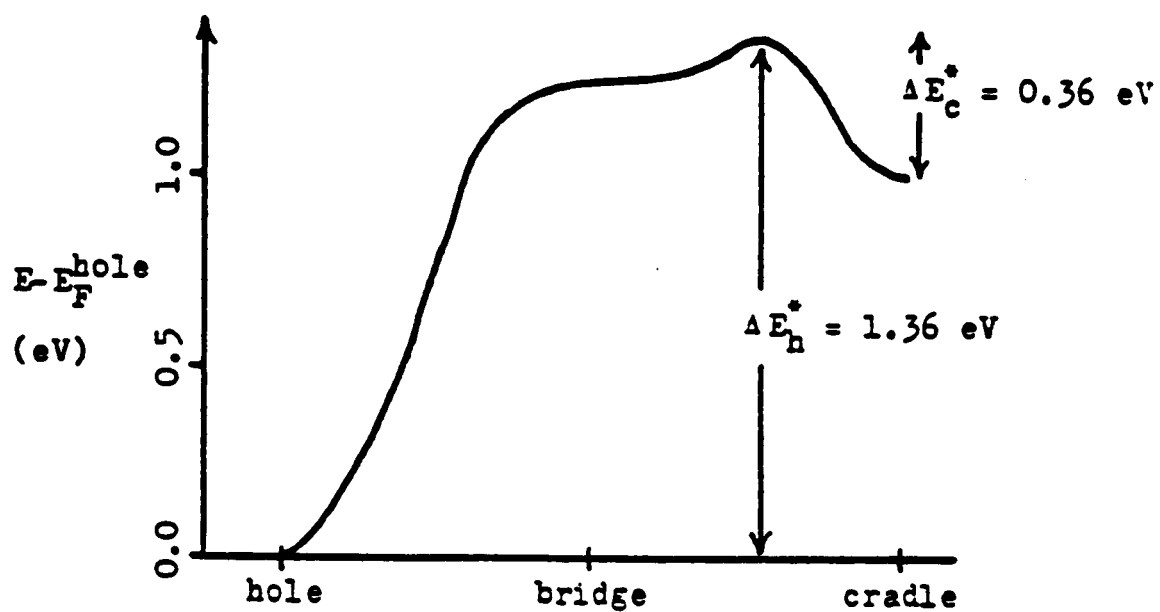


FIGURE 3

~~PRECEDING PAGE BLANK NOT FILLED~~

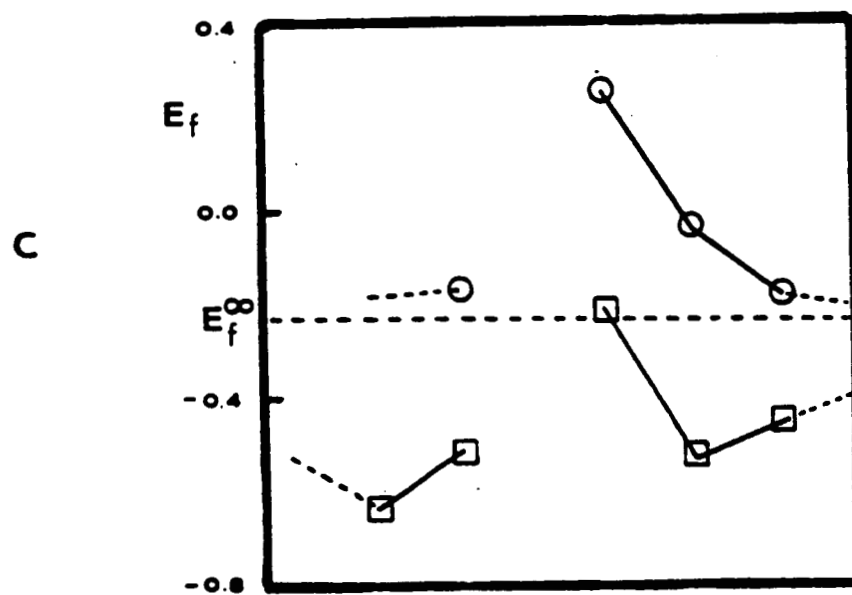
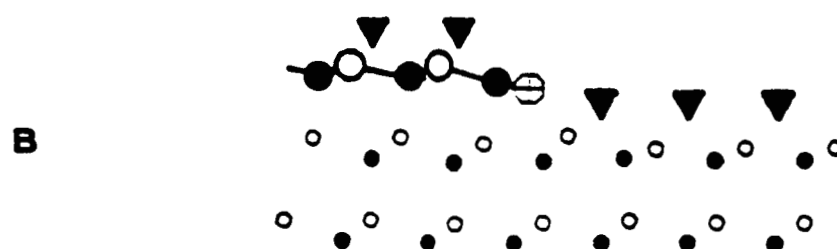
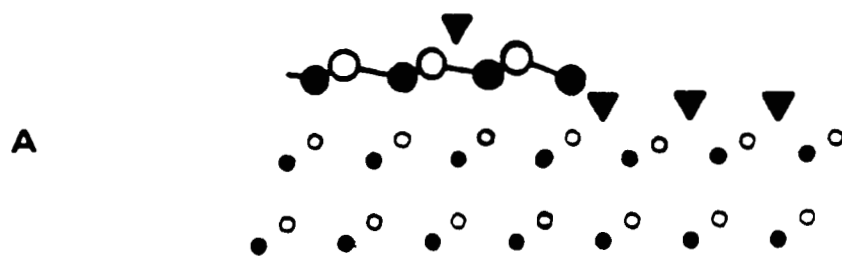


FIGURE 4

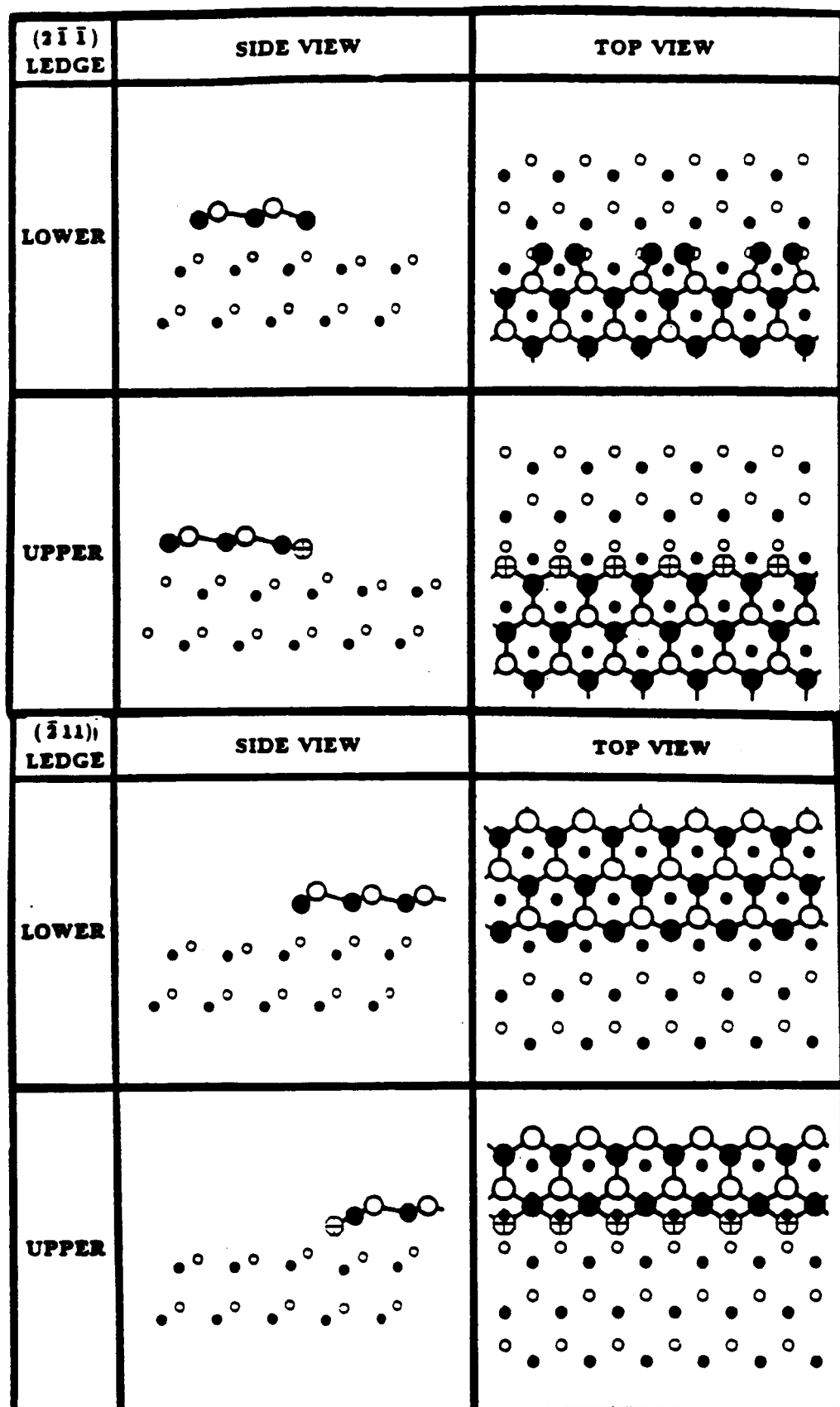


FIGURE 5

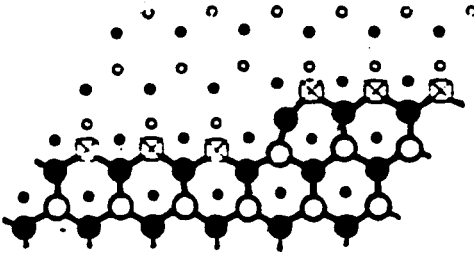
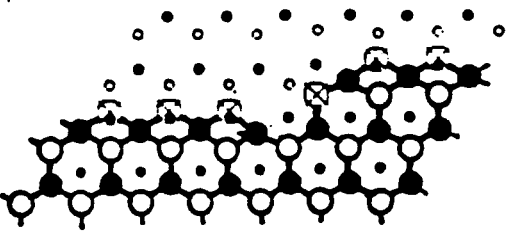
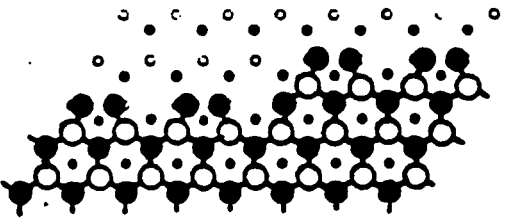
Ledge	λ_{oc}	E_K	Top View of Structure
$(2\bar{1}\bar{1})$ UPPER	0.01	0.75	
$(\bar{2}11)$ UPPER	0.01	0.73	
$(2\bar{1}\bar{1})$ LOWER	0.24	0.20	

FIGURE 6